

Article

# Mechanical Alloying as an Effective Way to Achieve Superior Properties of Fe–Co–Ni Binder Alloy

Pavel Loginov <sup>\*</sup>, Daria Sidorenko , Marina Bychkova , Mikhail Petrzhik and Evgeny Levashov

Scientific and Educational SHS Center MISIS-ISMAN, National University of Science and Technology “MISIS”, Leninsky prospect 4, 119049 Moscow, Russia; dsidorenko@inbox.ru (D.S.); bychkova@shs.misis.ru (M.B.); petrzhik@shs.misis.ru (M.P.); levashov@shs.misis.ru (E.L.)

\* Correspondence: pavel.loginov.misis@list.ru; Tel.: +7-916-695-6807

Received: 22 November 2017; Accepted: 11 December 2017; Published: 17 December 2017

**Abstract:** This study addresses the fabrication of nanocrystalline Fe–Co–Ni alloy using two operations: mechanical alloying (MA) of elemental powders and hot pressing (HP). The evolution of the phase composition and structure of the powder particles after MA was investigated. Ball milling with rotation speed 700 rpm for 15–20 min allows the production of a bcc Fe-based supersaturated solid solution. During the HP of this powder, this solution decomposes into a bcc (Fe) solid solution and fcc Fe<sub>3</sub>Ni precipitates, which act as a recrystallization barrier at elevated temperatures. This factor, along with the solid solution strengthening of the ( $\alpha$ -Fe) matrix and high concentration of lattice defects (dislocations and twins), provides high mechanical properties (ultimate bending strength of 2000 MPa and hardness of 108 HRB) and wear resistance of the alloy. The developed Fe–Co–Ni alloy is promising for use as a binder in diamond tools designed for machining abrasive materials.

**Keywords:** nanostructured materials; precipitation; strength; mechanical alloying/milling; transmission electron microscopy (TEM)

## 1. Introduction

Diamond tools are widely used in the construction and mining industries. The working layer of these tools is typically made of a composite material: diamond grains (or any other ultrahard materials such as cubic boron nitride) surrounded by the metal matrix (the binder). The diamond cuts the machined material due to repeated microscratching. The binder has several important functions: it holds the diamond in the working layer, is responsible for the redistribution of the bearing load, and ensures the conditions for working layer renewal (the wear rate of the binder being equal to that of diamond), which constantly maintains the high-performance properties of the tools [1].

Designing novel economical compositions of binders and the methods to prepare them is a topical trend in the development of diamond tools [2–4]. Co has been conventionally considered to be the best material for manufacturing binders due to the combination of high mechanical properties and wear resistance as well as its ability to firmly hold diamond grains within the working layer [1,5]. Nevertheless, its high cost and toxicity have forced tool manufacturers to seek other materials to fabricate binders that possess similar parameters [6,7]. This problem has been partially solved by using low-cobalt or cobalt-free alloys based on Fe, Ni, and Cu with physical, chemical, and mechanical properties that are similar to those of Co [8–10]. Binders for cutting tools with strength not inferior to Co have been designed by varying the compositions in Fe–Cu–Co [11], Fe–Cu–Sn [12], Fe–Ni–Cu–Sn–C [13], and Ni–Cr–P [14] systems and selecting the optimal mixing and compaction regimes.

To be able to use diamond tools with a low-cobalt binder for cutting and grinding highly abrasive materials, such as concrete, sandstone, and refractory materials, one needs to considerably enhance

the strength and wear resistance of these binders. In some cases, this is achieved by adding WC or Mo to the binder [1,15]. An alternative reinforcement method is to form a nanomodified or nanocrystalline structure without changing the chemical composition. This approach can be used under conditions of severe plastic deformation of a powder mixture followed by hot pressing (HP) at relatively low temperatures and for small treatment durations.

Mechanical alloying (MA) in planetary ball mills (PBMs) is an efficient method for preparing multicomponent mixtures with nanocrystalline and amorphous phases including those made of the components with a limited mutual solubility [16–19]. Metastable phases, such as supersaturated solid solutions, are formed in this case [20,21]; their decomposition upon heating is accompanied by the precipitation of the dispersed secondary phases. Also, MA is a well-proven method for production of powder mixtures with specific structure, for example, laminate one [22]. A crucial advantage of MA over other methods for preparing powder binders (e.g., chemical co-precipitation of metal hydroxide followed by its reduction [2]) is that the equipment used is rather simple.

This study aimed at fabricating nanocrystalline low-cobalt Fe–Co–Ni binders with high mechanical properties and wear resistance to be used in diamond tools for cutting highly abrasive materials. To meet this objective, we studied the features of the phase and structure formation during MA of powder mixtures and elucidated the properties and the mechanisms of material strengthening.

It should be mentioned that the MA of Fe–Co–Ni powder mixtures was previously used to synthesize materials with special magnetic properties [23–25]. The possibility of significantly enhancing the strength and wear resistance has not yet been described in the literature.

## 2. Materials and Methods

Carbonyl Fe powder (Sintez-PKZh LLC, Dzerzhinsk, Russia; mean grain size, 9  $\mu\text{m}$ ; impurity content  $\leq 0.3$  wt. %), carbonyl Ni powder (AO Kola Mining and Metallurgical Company, Monchegorsk, Russia; mean grain size, 10  $\mu\text{m}$ ; impurity content  $\leq 0.06$  wt. %), and reduced Co powder (Nanjing Hanrui Cobalt Co. Ltd., Nanjing, China; mean grain size, 1.2  $\mu\text{m}$ ; impurity content  $\leq 0.03$  wt. %) were used as the initial materials. The chemical composition of powder mixtures was constant—75% Fe, 15% Co and 10% Ni (mass. %).

Powder mixtures were prepared using two types of setups. Grains of various components were mechanically mixed in a Turbula mixer (Vibrotekhnik LLC, Moscow, Russia) for 60 min.

To produce MA mixtures, the mixtures were treated in an Activator-2s laboratory planetary ball mill (PBM) (Engineering Plant “Activator” LLC, Novosibirsk, Russia). The duration of MA varied in the range from 5 to 20 min. Other parameters were constant: carrier rotation speed, 700 rpm; centrifugal factor, 120 g. The drums were filled with Ar to prevent oxidation of the charge mixture during treatment.

Compacted samples had a shape of right parallelepiped ( $10 \times 10 \times 0.3$  cm<sup>3</sup> in size) were prepared from the powder mixtures by hot pressing (HP) after 0, 5, 10, 15, and 20 min of MA (one for each MA regime). The HP temperature was 950 °C; pressure at the maximum temperature was 35 MPa, and the exposure time was 3 min. These preforms were used to cut out samples to measure the ultimate bending strength, hardness, and porosity. The residual porosity of the compacted samples was determined by hydrostatic weighing on an analytical balance (A&D, Tokyo, Japan). Weights were measured to an accuracy of 0.1 mg.

The ultimate bending strength was measured on an LF-100 servo-hydraulic universal testing machine (Walter + bai, Löhningen, Switzerland) with an external digital controller (EDC). The ultimate bending strength values were determined using the DIONPro software (V.4.10, Walter + bai, Löhningen, Switzerland) enabling automated registration and statistical processing of the test results. Six samples for the tests with dimensions  $7 \times 1 \times 0.3$  cm<sup>3</sup> were prepared from HP compacts using electric discharge sawing.

The Rockwell hardness was tested using a Wolpert Rockwell Hardness Tester (Wolpert 600 MRD, Aachen, Germany). Furthermore, the mechanical properties (hardness H and Young's

modulus E) of certain phases, contained within hot-pressed samples, were determined using a high-precision nano-hardness tester (CSM Instruments, Peseux, Switzerland) according to the Oliver–Pharr method [26]. A diamond three-sided pyramid (a Berkovich tip) was used as an indenter. The indentation load was 10 mN; the loading speed was 0.36 mN/s; the time of exposure to the maximum load was 5 s. Nanoindentation testing was performed with an increment of 20 and 15  $\mu\text{m}$  towards the X- and Y-axes, respectively. The matrix consisted of 100 indents.

X-ray powder diffraction (XRD) analysis was performed on an automated DRON 4-07 X-ray diffractometer (Burevestnik R&D Company, St. Petersburg, Russia) using monochromated Co-K $\alpha$  radiation in the Bregg–Brentano geometry. A graphite monochromator was used to monochromatize radiation. Lattice parameters were measured with a relative error of  $\Delta a/a = 0.0001$  nm/nm.

The structures of the powder and compacted materials were studied using scanning electron microscopy on an S-3400N microscope (Hitachi, Tokyo, Japan) equipped with a NORAN energy-dispersive X-ray spectrometer. Fine-structure features of the samples were studied by transmission electron microscopy using a JEOL JEM 2100 microscope (JEOL Ltd., Tokyo, Japan). Samples that were  $5 \times 3 \mu\text{m}^2$  in size were prepared using a focused ion beam.

The friction coefficient and the reduced wear of the samples were determined using the rolling sliding wear test on an automated tribometer machine (CSM Instruments, Peseux, Switzerland) using the rod-on-disk scheme under the following conditions: the wear track radius was 6.8 mm; the applied load was 2 N; the maximum speed was 10 cm/s; a ball 3 mm in diameter made of sintered  $\text{Al}_2\text{O}_3$  was used as a counterbody; the path was 214 m (5000 cycles); and air was used as the medium. The fractographic examination of the wear tracks on the samples was carried out by optic profilometry using a WYKO NT1100 optical profiler (Veeco, Plainview, NY, USA).

### 3. Results and Discussion

#### 3.1. Mechanical Alloying of the Fe–Co–Ni Powder Mixture

XRD patterns recorded for the Fe–Co–Ni powder mixtures treated in the Turbula mixer and in the PBM for different times were examined to analyse the features of the phase formation during MA.

Figure 1 demonstrates that the XRD pattern of the Turbula mixture contains diffraction peaks from the  $\alpha$ -Fe, Co (hcp crystal structure), and Ni phases. The mean size of the coherent scattering regions (CSRs) for the phases was greater than 500 nm. The XRD pattern of the mixture prepared using MA with a minimum exposure time (five min) shows peak broadening indicating that grains were refined and disintegrated into subgrains [27]. The small shift in peaks from the  $\alpha$ -Fe phase towards greater  $2\theta$  angles and the significant reduction in the intensity of the peaks from Co demonstrate that Co was dissolved in the  $\alpha$ -Fe [28]. Despite the dissolution of dopants, the lattice parameter of the  $\alpha$ -Fe phase changed negligibly (Table 1). The reason for this is that the percentage of the dissolved components was small during the initial stage of MA and because of the insignificant difference between the atomic radii of Fe, Co, and Ni (126, 125, and 124 pm, respectively) [29]. After the duration of MA had been increased (10–15 min), Co was completely dissolved in the  $\alpha$ -Fe phase, and the dissolution of Ni in  $\alpha$ -Fe was more intense. In the XRD patterns of these powder mixtures, the peaks from Ni shifted towards smaller  $2\theta$  angles demonstrating that the lattice parameter of this phase increased and Fe was dissolved in this phase [30]. Only ( $\alpha$ -Fe) phase remains in the powder mixture after MA for 20 min. Since this composition in the equilibrium state is two-phase, it can be inferred that this phase is a supersaturated solid solution.

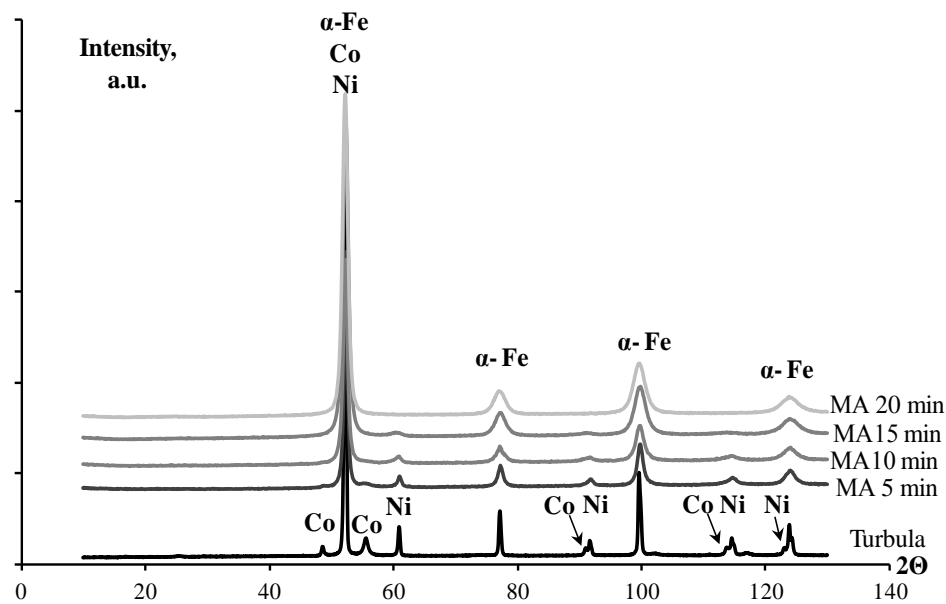


**Figure 1.** X-ray powder diffraction (XRD) patterns of the Fe–Co–Ni powder mixtures prepared in the Turbula mixer and mechanically alloyed in the planetary ball mill (PBM).

**Table 1.** Phase composition of the Fe–Co–Ni powder mixtures.

Sample	Phase								
	α-Fe cI2/1			Co hP2/1			Ni cF4/1		
	Wt. %	Cr. Size, nm	Lattice Parameter, nm	Wt. %	Cr. Size, nm	Lattice Parameter, nm	Wt. %	Cr. Size, nm	Lattice Parameter, nm
Turbula	76	>500	0.2866	8	-	A = 0.2507 C = 0.4078	16	>500	0.3525
Mechanical alloying (MA) 5 min	84	51	0.2865	3	-	-	13	75	0.3525
MA 10 min	90	35	0.2865	-	-	-	10	30	0.3532
MA 15 min	98	22	0.2865	-	-	-	2	-	0.3551
MA 20 min	100	19	0.2866	-	-	-	-	-	-

The initial Fe and Ni powders had a near-spherical shape and were 5–10  $\mu\text{m}$  in size. Co grains that were one micrometer in size had a dendritic shape. The mixture prepared in the Turbula mixer was a combination of these grains homogeneously distributed over the volume (Figure 2a).

Grains with the lamellar structure were formed during MA of the Fe–Co–Ni mixture, which is typical for “ductile–ductile” systems [31]. The powders were deformed after colliding with the grinding media, and large composite granules were formed as a result of the cold-welding process (Figure 2b). The thickness of the alternating layers varied between 1  $\mu\text{m}$  and 10  $\mu\text{m}$ . The layer thickness decreased as the MA duration increased to 10 min (Figure 2c); a homogeneous structure was formed after MA for 15 min (Figure 2d). Further increases in the MA duration had no effect on the structure.

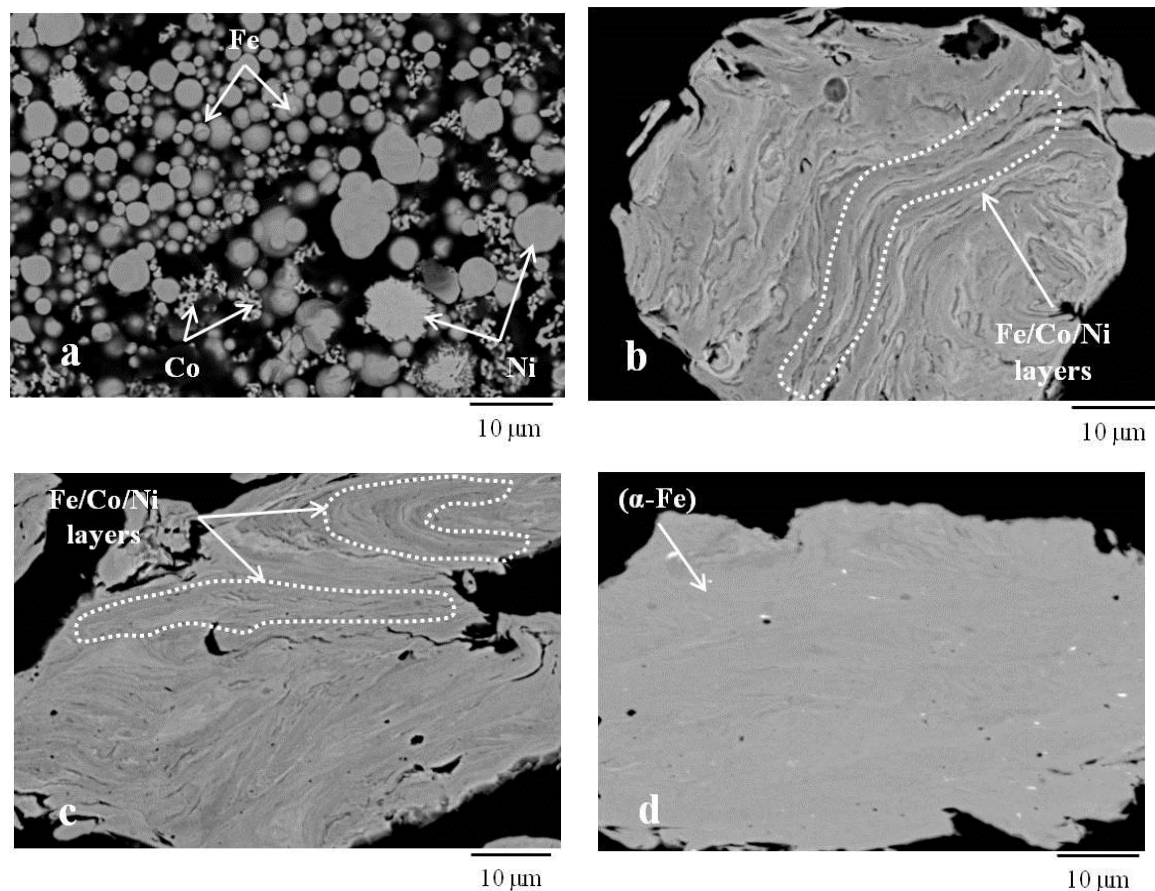


**Figure 2.** Structures of the Fe–Co–Ni powder mixtures after being mixed: (a) in the Turbula mixer; (b) after MA in the PBM for 5 min; (c) 10 min; (d) 15 min.

### 3.2. Structure and Mechanical Properties of the Hot-Pressed Fe–Co–Ni Samples

Compacted samples were obtained from the Fe–Co–Ni powder mixtures prepared in both types of mixers; their physical and mechanical properties were studied. Table 2 demonstrates that MA increased the hardness and the ultimate bending strength of the samples by 20% and 55%, respectively. The dependences of the mechanical properties on the MA duration increased continuously up to the MA duration of 15 min. The same mechanical properties for the MA duration of 15 and 20 min is explained by the fact that mixtures had been completely attained after 15 min of MA.

**Table 2.** Physical and mechanical properties of the Fe–Co–Ni hot-pressed samples.

Sample	Porosity, %	Hardness, HRB	Ultimate Bending Strength, MPa
Turbula	3.6	$89 \pm 1$	$1272 \pm 6$
MA 5 min	3.0	$105 \pm 1$	$1731 \pm 20$
MA 10 min	3.2	$105 \pm 1$	$1855 \pm 9$
MA 15 min	3.3	$107 \pm 1$	$1980 \pm 69$
MA 20 min	3.6	$108 \pm 1$	$1944 \pm 57$

Strengthening the Fe–Co–Ni binder using the MA mixtures was ensured due to several mechanisms: formation of the nanocrystalline structure, solid solution strengthening, and high density of dislocations and other lattice defects.

Two microstructures were observed in the samples hot-pressed from the Turbula mixture: grains of the Ni phase were surrounded by the ( $\alpha$ -Fe) matrix (Figure 3a). Ni grains had a nearly equiaxial

shape, and their size corresponded to that of the initial Ni powder (10  $\mu\text{m}$ ). The X-ray powder diffraction studies showed that solid solutions based on iron ( $\alpha\text{-Fe}$ ) and nickel Ni were present (Table 3). The deviation of the lattice parameter of Ni from the reference value ( $a = 0.3524$  nm) indicates that Fe and Co were dissolved at the interface with the ( $\alpha\text{-Fe}$ ). However, Ni grains in the central part were not involved in the interaction. The XRD patterns contained no peaks characteristic of Co, which confirms that it dissolved in the ( $\alpha\text{-Fe}$ ) lattice during hot pressing.

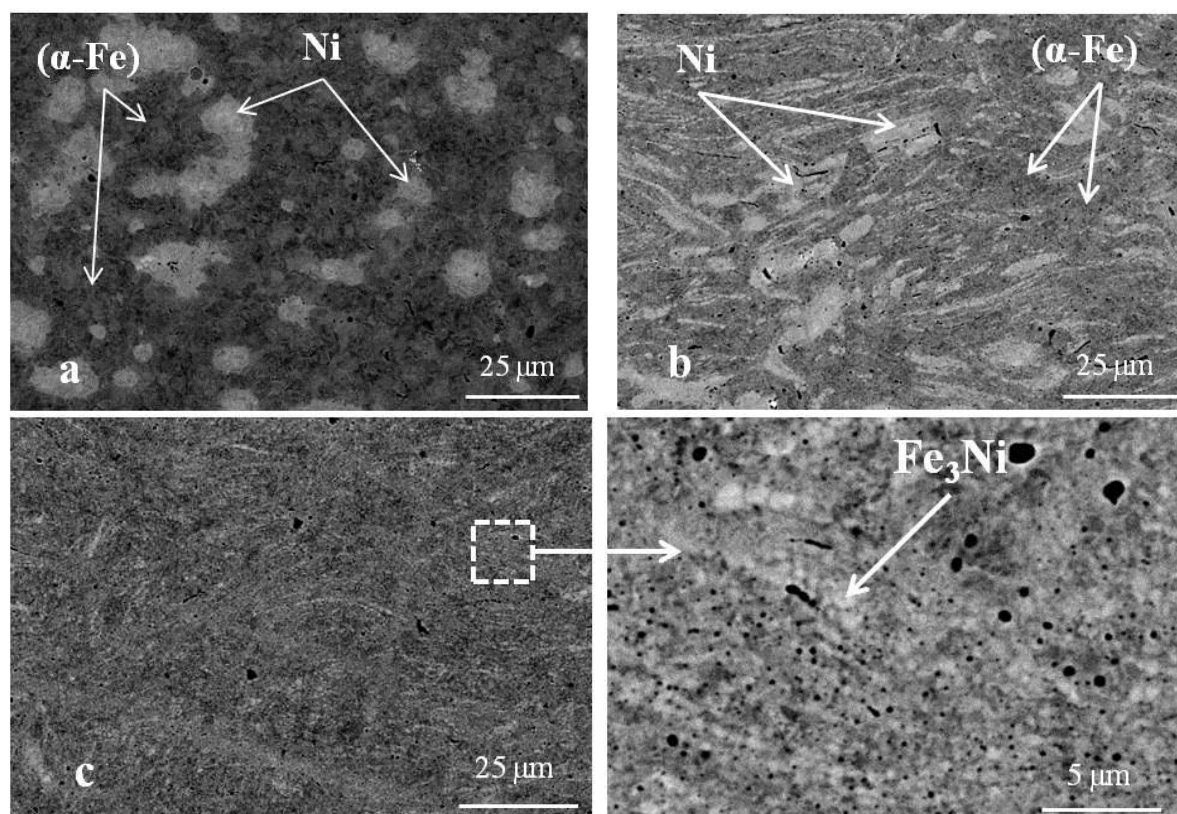


**Figure 3.** The structure of the hot-pressed Fe–Co–Ni samples obtained from the powder mixtures prepared: (a) in the Turbula mixer; (b) mechanically alloyed in PBM for 5 and (c) 10 min.

**Table 3.** Phase composition of the hot-pressed Fe–Co–Ni samples.

Sample	Phase					
	$(\alpha\text{-Fe})$ cI2/1		Ni cF4/1		$\text{Fe}_3\text{Ni}$ cF4/1	
	wt. %	$a$ , nm	wt. %	$a$ , nm	wt. %	$a$ , nm
Turbula	87	0.2867	13	0.3554	-	-
MA 5 min	90	0.2869	10	0.3581	-	-
MA 10 min	92	0.2866	-	-	8	0.3596
MA 15 min	94	0.2866	-	-	6	0.3594
MA 20 min	94	0.2866	-	-	6	0.3594

The samples prepared from the MA mixture (five min) inherited the lamellar structure from the powder mixture. Ni grains were oblong and had the mean thickness of three to five micrometers (Figure 3b). The contact surface area between the components increased due to intense plastic deformation during MA. This intensified the diffusion processes at the interface and caused dissolution of Ni in the ( $\alpha\text{-Fe}$ ) (Table 3).

The lamellar distribution of the Ni phase was also observed in the structure of the samples hot-pressed from the mixtures subjected to MA for 10 min (Figure 3c). This phase has a fcc lattice ( $a = 0.3596$  nm) (Table 3), which is much greater than that of pure Ni and the Ni-based solid solution that was present in the mixture before hot pressing (Table 1). The difference in the lattice parameters was attributed to the different mechanism of phase formation. This phase was probably the secondary phase that was precipitated from the supersaturated solid solution ( $\alpha$ -Fe) during hot pressing. This phase is close to the  $\text{Fe}_3\text{Ni}$  phase in terms of its lattice parameters [32] and has a similar chemical composition (shown below).

The structure of the powder mixtures samples subjected to MA for 15 min includes homogeneously distributed grains of the ( $\alpha$ -Fe) matrix and the secondary  $\text{Fe}_3\text{Ni}$  phase with an average size of 300 nm (Figure 4). This structure can be obtained in the compacted material due to the nanocrystalline structure of the powders from which it is made (Table 1). In addition, the crystal lattice of the grains of the secondary  $\text{Fe}_3\text{Ni}$  phase was incoherent with respect to the ( $\alpha$ -Fe) matrix (Figure 5). Therefore, the precipitated secondary phase prevents the migration of grain boundaries at hot pressing temperatures and acts as a recrystallization barrier.

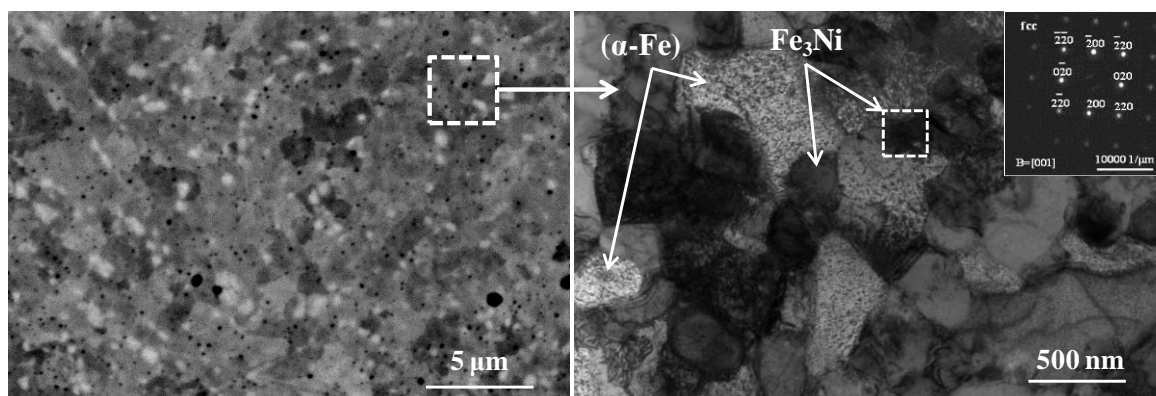


**Figure 4.** The nanocrystalline structure of the hot-pressed sample of the Fe–Co–Ni mixture after MA for 15 min.

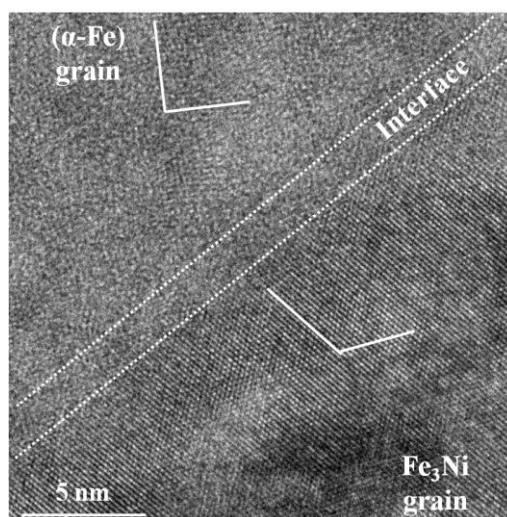


**Figure 5.** A high resolution transmission electron microscopy (TEM) image of the interface demonstrating that the crystal lattice of  $\alpha$ -Fe and secondary  $\text{Fe}_3\text{Ni}$  grains are non-coherent.

High-energy treatment of the Fe–Co–Ni powder mixture in the PBM resulted in complete dissolution of Ni and Co in the ( $\alpha$ -Fe) lattice. Therefore, the solid-solution strengthening effect can be expected in hot-pressed materials. To determine the contribution of this strengthening mechanism, we studied the structure and the chemical composition of the alloy and measured the mechanical properties of the individual structural components using a nanoindentation test.

The samples prepared from the Turbula mixtures were characterized by heterogeneous element distribution due to the short duration of hot pressing and limited mutual solubility of the components in the Fe–Ni and Fe–Co systems. As a result, the structure contained individual Fe and Ni grains, while the solid solution was formed only at the interface between them (Figure 6). The EDX study of the local elemental composition showed that the central zones of these grains contained almost no dopants (Table 4).

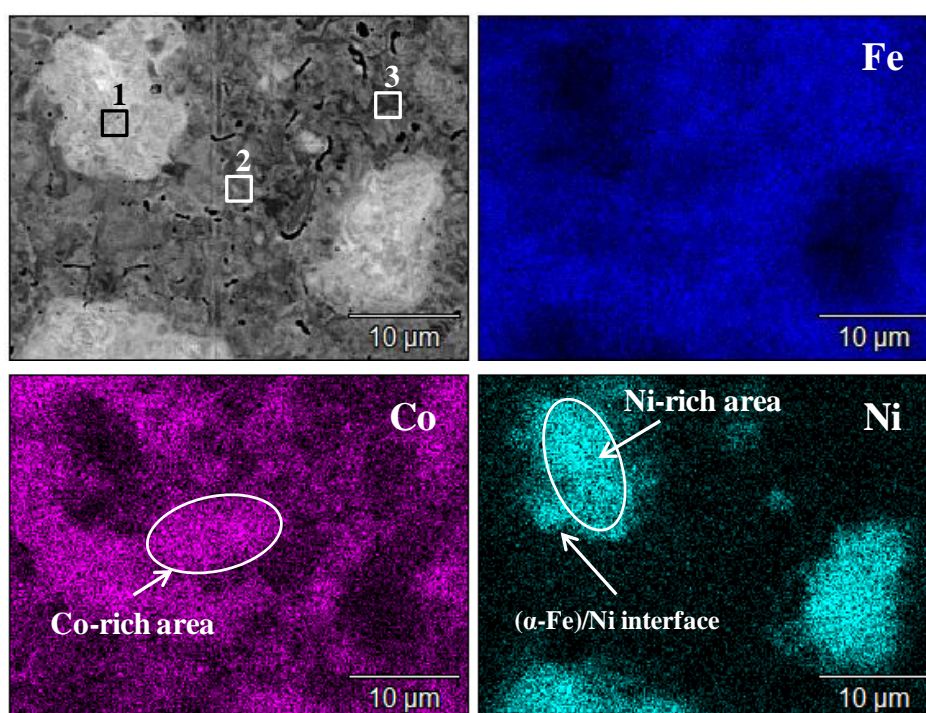


**Figure 6.** Element distribution maps in the hot-pressed Fe–Co–Ni samples made of the powder mixture prepared in the Turbula mixer.

**Table 4.** Elemental composition of different areas in the hot-pressed Fe–Co–Ni samples made from the Turbula mixture and the mixture subjected to MA for 15 min.

Turbula	Fe, wt. %	Co, wt. %	Ni, wt. %
Spot 1 (Figure 6)	16	5	79
Spot 2 (Figure 6)	55	45	-
Spot 3 (Figure 6)	88	12	-
MA 15 min			
Spot 4 (Figure 7)	78	13	9
Spot 5 (Figure 7)	75	10	15
Spot 6 (Figure 7)	75	10	15

The elemental composition of the grains in the Fe–Co–Ni samples that were hot-pressed from the MA mixture (15 min) was determined using a combination of TEM and EDX. The high accuracy of the

measurement in this experiment was assured by the small thickness of the test sample (a lamella <100 nm thick) and electron beam diameter  $\leq 50$  nm.

As shown in Figure 7, this sample contained two structural components corresponding to the ( $\alpha$ -Fe) and Fe<sub>3</sub>Ni phases. Both of these phases were structurally complex alloyed phases. The average composition of the ( $\alpha$ -Fe) grains was found to be (wt. %) 78% Fe, 13% Co, and 9% Ni. Grains of the secondary phase were characterized by a greater Ni concentration and contained dissolved Co (Table 4). An analysis of several Fe<sub>3</sub>Ni grains showed that their elemental compositions were identical.

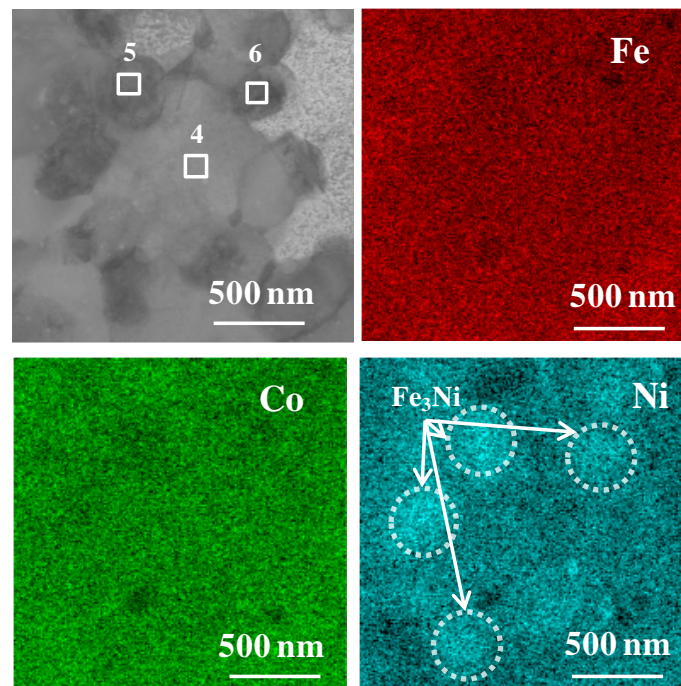


**Figure 7.** Element distribution maps in the hot-pressed Fe–Co–Ni samples made of the powder mixture subjected to MA for 15 min.

The contribution of solid solution strengthening to enhance the mechanical properties of the alloy was qualitatively assessed by nanoindentation. The load was selected so that the surface area of the indent was smaller than the size of a single grain. The dissolution of a large amount of dopants in the ( $\alpha$ -Fe) phase caused its hardness to increase by 20% (4.8 and 4.0 GPa, respectively, Table 5). This can be seen from the decrease in the indenter penetration depth during the tests (Figure 8).

**Table 5.** Mechanical properties of the individual structural components in the hot-pressed Fe–Co–Ni samples made from the Turbula mixture and the mixture subjected to MA for 15 min (R—elastic recovery).

Sample	( $\alpha$ -Fe)			(Ni)/Fe <sub>3</sub> Ni			Bulk Sample		
	H, GPa	E, GPa	R, %	H, GPa	E, GPa	R, %	H, GPa	E, GPa	R, %
Turbula	4.0 $\pm$ 0.2	241 $\pm$ 14	11.83	5.0 $\pm$ 0.3	260 $\pm$ 6	15.06	4.2 $\pm$ 1.0	244 $\pm$ 16	12.25
MA 15 min	4.8 $\pm$ 0.3	225 $\pm$ 15	15.20	5.8 $\pm$ 0.4	231 $\pm$ 8	18.21	5.1 $\pm$ 0.6	227 $\pm$ 14	15.77

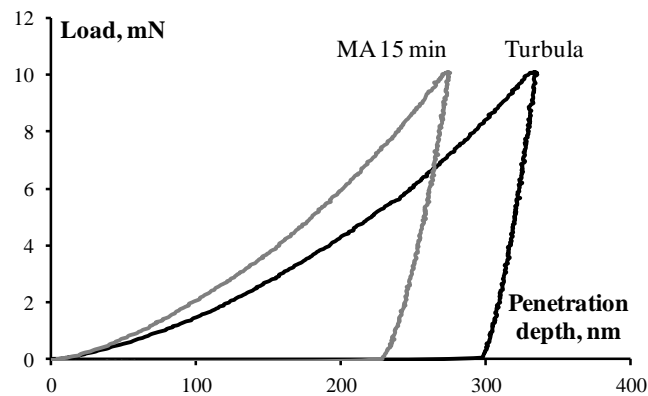


**Figure 8.** Indentation curves of the ( $\alpha$ -Fe) phase grains in the hot-pressed Fe–Co–Ni samples made from Turbula mixture and the mixture subjected to MA for 15 min.

A large number of crystal lattice defects accumulated in the Fe–Co–Ni powder particles during high-energy treatment in the PBM. This can be seen from the decrease in crystallite size (Table 1) and occurred under severe plastic deformation accompanying the formation of the complex alloyed and metastable phases [33].

Hot pressing of the mixture subjected to MA for three minutes at the maximum temperature of 950 °C did not annihilate the dislocations, nor did it appear to grossly change their distribution or their embedment into the walls. The high dislocation concentration in ( $\alpha$ -Fe) grains was confirmed by the TEM images of the structure (Figure 9a). Furthermore, it was previously ascertained that hot pressing of MA mixtures made grains of the secondary  $\text{Fe}_3\text{Ni}$  phase precipitate. Twin defects began to form in  $\text{Fe}_3\text{Ni}$  as a result of external loads (Figure 9b), which is typical of the materials crystallizing in the fcc system [34]. Twin boundaries reduced the space and impeded the dislocation motion [35]. These factors combined to ensure strengthening of the material.



**Figure 9.** Crystal lattice defects in the hot-pressed Fe–Co–Ni samples made from the mixtures subjected to MA for 15 min: dislocations (a) (shown with arrows) and twin boundaries (b).

### 3.3. Results of Wear Tests

Operating time is one of the key characteristics of diamond cutting tools. This shows the ratio between the machined surface area and the weight loss of the tool working layer. The specific operating time of a tool is typically affected by the wear resistance of the binder. Therefore, to assess the operating time of the tool, we performed tribological tests simulating real-life conditions. The mechanical properties of the counterbody material (sintered alumina) were close to those of concrete. Polished samples of hot-pressed Fe–Co–Ni binders made of the powders prepared in the Turbula mixer and MA in the PBM with different treatment duration were used as test objects.

The tests showed that the wear resistance of the samples prepared using the MA mixtures was twofold to threefold greater (Figure 10). The optimal duration of the MA for the Fe–Co–Ni powder mixtures was shown to be 15 min. The samples prepared in this regime were characterized by a relatively low wear ( $4.5 \times 10^{-5} \text{ mm}^3/\text{N}/\text{m}$ ), as shown in Table 6.

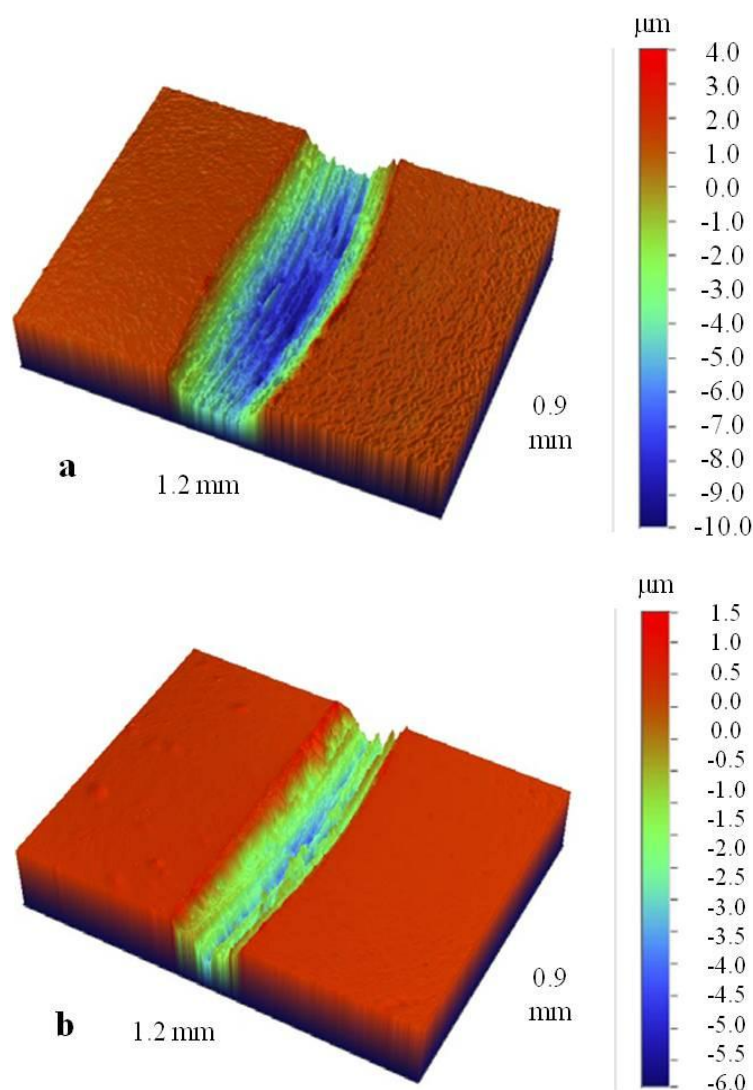


**Figure 10.** Three-dimensional profiles of the wear tracks of the hot-pressed Fe–Co–Ni samples made from the (a) Turbula mixture and (b) the mixture subjected to MA for 15 min.

**Table 6.** Tribological characteristics of the hot-pressed Fe–Co–Ni binders.

Sample	Wear, $10^{-5}$ mm <sup>3</sup> /N/m	Mean Friction Coefficient
Turbula	14.6	0.51
MA 5 min	9.8	0.76
MA 10 min	7.0	0.66
MA 15 min	4.5	0.48
MA 20 min	4.6	0.58

#### 4. Conclusions

1. The features of the phase and structure formation during mechanical alloying of Fe–Co–Ni powder mixtures were studied. A supersaturated solid solution based on  $\alpha$ -Fe could be prepared after MA for  $\geq 15$  min.
2. The structure and the phase composition of a powder mixture were shown to significantly affect the mechanical properties of the sintered binder. The samples prepared from the MA mixtures had a 20% greater hardness (up to 108 HRB) and 55% greater ultimate bending strength (up to 2000 MPa). This effect was achieved from the following strengthening mechanisms:
  - Formation of a nanocrystalline structure during MA and its retention in the compacted samples;
  - Solid solution strengthening of the ( $\alpha$ -Fe) matrix resulting from the precipitation of grains from the secondary Fe<sub>3</sub>Ni phase that were incoherent with respect to the matrix, which impedes grain recrystallization;
  - High concentration of crystal lattice defects: dislocations in the ( $\alpha$ -Fe) phase grains and twin defects in the Fe<sub>3</sub>Ni phase grains.

The combination of high mechanical properties and wear resistance makes nanocrystalline mechanically alloyed Fe–Co–Ni binders promising for use in diamond cutting tools for machining abrasive materials.

**Acknowledgments:** This work was carried out with partial financial support from the Russian Foundation for Basic Research and Moscow Government in the framework of project (No. 15-38-70019 «mol\_a\_mos») in the part of studying the strengthening mechanism in MA Fe–Co–Ni binders and the Ministry of Education and Science of the Russian Federation in the framework of Increase Competitiveness Program of NUST “MISiS”: (No. K2-2016-073) in the part of investigation of wear resistance of nanocrystalline binders.

**Author Contributions:** Pavel Loginov performed most of experiments and wrote this manuscript; Daria Sidorenko helped with preparation of experimental equipment and specimens for electron microscopy and tensile tests; Marina Bychkova helped to analyze the experimental data and gave some constructive suggestions; Mikhail Petrzhhik helped with some experiments and discussion of the results; Evgeny Levashov participated in the results discussion and guided the writing of the article.

**Conflicts of Interest:** The authors declare no conflict of interest.

#### References

1. Konstanty, J. *Powder Metallurgy Diamond Tools*; Elsevier: Oxford, UK, 2005; pp. 123–125. ISBN 1-856-17440-9.
2. Jahani, M.; Sattari, S.; Atrian, A. Effect of volume fraction of reinforcement and milling time on physical and mechanical properties of Al7075–SiC composites fabricated by powder metallurgy method. *Powder Metall. Ceram.* **2017**, *56*, 283–292. [[CrossRef](#)]
3. Oliveira, F.A.C.; Anjinho, C.A.; Coelho, A.; Amaral, P.M.; Coelho, M. PM materials selection: The key for improved performance of diamond tools. *Met. Powder Rep.* **2017**, *27*, 339–344. [[CrossRef](#)]
4. Brookes, K. Longer-lasting low-cost diamond tools. *Met. Powder Rep.* **2012**, *67*, 30–33. [[CrossRef](#)]
5. Molinari, A.; Marchetti, F.; Gialanella, S.; Scardi, P.; Tiziani, A. Study of the diamond-matrix interface in hot-pressed cobalt-based tools. *Mat. Sci. Eng. A* **1990**, *130*, 257–262. [[CrossRef](#)]

6. Oliveira, H.C.P.; Cabral, S.C.; Guimarães, R.S.; Filgueira, M. Is Ni a good substitute for Co in PM diamond cutting tools? *Mater. Sci. Forum* **2010**, *660–661*, 363–369. [[CrossRef](#)]
7. Oliveira, H.C.P.; Coelho, A.; Amaral, P.M.; Fernandes, J.C.; Rosa, L.G. Comparison between cobalt and niobium as a matrix component for diamond impregnated tools used for stone cutting. *Key Eng. Mater.* **2013**, *548*, 98–105. [[CrossRef](#)]
8. Oglezneva, S.A. Diamond tools with metastable steel binder for natural stone cutting. *J. Frict. Wear* **2011**, *32*, 313–317. [[CrossRef](#)]
9. Romanski, A.; Konstanty, J.; Ratuszek, W. New Fe-Ni and Fe-Mn powders used in manufacturing diamond tools. *Appl. Mech. Mater.* **2013**, *431*, 3–7. [[CrossRef](#)]
10. Tan, S.; Fang, X.; Yang, K.; Duan, L. A new composite impregnated diamond bit for extra-hard, compact, and nonabrasive rock formation. *Int. J. Refract. Met. Hard Mater.* **2014**, *43*, 186–192. [[CrossRef](#)]
11. Barbosa, A.P.; Bobrovnitchii, G.S.; Skyry, A.L.; Guimars, R.S.; Filgueira, M. Structure, microstructure and mechanical properties of PM Fe–Cu–Co alloys. *Mater. Des.* **2010**, *31*, 522–526. [[CrossRef](#)]
12. Konstanty, J.; Tyrala, D. Wear mechanism of iron-base diamond-impregnated tool composites. *Wear* **2013**, *303*, 533–540. [[CrossRef](#)]
13. Konstanty, J.; Romanski, A.; Tyrala, D. Ferrous ball-milled powders for the fabrication of sintered diamond tools. *Adv. Mat. Res.* **2014**, *1052*, 514–519. [[CrossRef](#)]
14. Wang, C.Y.; Zhou, Y.M.; Zhang, F.L.; Xu, Z.C. Interfacial microstructure and performance of brazed diamond grits with Ni–Cr–P alloy. *J. Alloy. Compd.* **2009**, *476*, 884–888. [[CrossRef](#)]
15. Andreev, V.A.; Gureev, A.I.; Sevast'yanov, P.I.; Loginov, V.I.; Levashov, E.A.; Loginov, P.A.; Rupasov, S.I.; Kurbatkina, V.V. Features of the influence of nanomodification and macrostructurization on the properties of the Fe-Mo binder for a diamond tool. *Russ. J. Non Ferr. Met.* **2014**, *55*, 652–656. [[CrossRef](#)]
16. Ibrahim, N.; Peterlechner, M.; Emeis, F.; Wegner, M.; Divinski, S.V.; Wilde, G. Mechanical alloying via high-pressure torsion of the immiscible Cu<sub>50</sub>Ta<sub>50</sub> system. *Mat. Sci. Eng. A* **2017**, *685*, 19–30. [[CrossRef](#)]
17. Azabou, M.; Ibn Gharsallah, H.; Escoda, L.; Suñol, J.J.; Kolsi, A.W.; Khitouni, M. Mechanochemical reactions in nanocrystalline Cu–Fe system induced by mechanical alloying in air atmosphere. *Powder Technol.* **2012**, *224*, 338–344. [[CrossRef](#)]
18. Contini, A.; Delogu, F.; Garroni, S.; Mulas, G.; Enzo, S. Kinetics behaviour of metastable equiatomic Cu-Fe solid solution as function of the number of collisions induced by mechanical alloying. *J. Alloy. Compd.* **2015**, *615*, S551–S554. [[CrossRef](#)]
19. Baláž, P.; Achimovicová, M.; Baláž, M.; Billik, P.; Zara, C.-Z.; Criado, J.M.; Delogu, F.; Dutková, E.; Gaffet, E.; Gotor, F.J.; et al. Hallmarks of mechanochemistry: From nanoparticles to technology. *Chem. Soc. Rev.* **2013**, *42*, 7571–7637. [[CrossRef](#)] [[PubMed](#)]
20. Prosviryakov, A.S.; Shcherbachev, K.D.; Tabachkova, N.Y. Microstructural characterization of mechanically alloyed Al-Cu-Mn alloy with zirconium. *Mat. Sci. Eng. A* **2015**, *623*, 109–113. [[CrossRef](#)]
21. Lei, R.S.; Wang, M.P.; Li, Z.; Wei, H.G.; Yang, W.C.; Jia, Y.L.; Gong, S. Structure evolution and solid solubility extension of copper–niobium powders during mechanical alloying. *Mat. Sci. Eng. A* **2011**, *528*, 4475–4481. [[CrossRef](#)]
22. Garroni, S.; Enzo, S.; Delogu, F. Mesostructural refinement in the early stages of mechanical alloying. *Scr. Mater.* **2014**, *83*, 49–52. [[CrossRef](#)]
23. Duan, Y.; Zhang, Y.; Wang, T.; Gu, S.; Li, X.; Lv, X. Evolution study of microstructure and electromagnetic behaviors of Fe–Co–Ni alloy with mechanical alloying. *Mat. Sci. Eng. B* **2014**, *185*, 86–93. [[CrossRef](#)]
24. Raanaei, H.; Eskandari, H.; Mohammad-Hosseini, V. Structural and magnetic properties of nanocrystalline Fe–Co–Ni alloy processed by mechanical alloying. *J. Magn. Magn. Mater.* **2016**, *398*, 190–195. [[CrossRef](#)]
25. Ahmadian Baghbaderani, H.; Sharafi, S.; Delshad Chermahini, M. Investigation of nanostructure formation mechanism and magnetic properties in Fe<sub>45</sub>Co<sub>45</sub>Ni<sub>10</sub> system synthesized by mechanical alloying. *Powder Technol.* **2012**, *230*, 241–246. [[CrossRef](#)]
26. Oliver, W.C.; Pharr, G.M. Improved technique for determining hardness and elastic modulus using load and displacement sensing indentation experiments. *J. Mater. Res.* **1992**, *7*, 1564–1580. [[CrossRef](#)]
27. Patil, U.; Hong, S.-J.; Suryanarayana, C. An unusual phase transformation during mechanical alloying of an Fe-based bulk metallic glass composition. *J. Alloy. Compd.* **2005**, *389*, 121–126. [[CrossRef](#)]
28. Loginov, P.A.; Levashov, E.A.; Kurbatkina, V.V.; Zaitsev, A.A.; Sidorenko, D.A. Evolution of the microstructure of Cu–Fe–Co–Ni powder mixtures upon mechanical alloying. *Powder Technol.* **2015**, *276*, 166–174. [[CrossRef](#)]

29. Hamzaoui, R.; Elkedim, O.; Gaffet, E. Milling conditions effect on structure and magnetic properties of mechanically alloyed Fe–10% Ni and Fe–20% Ni alloys. *Mat. Sci. Eng. A* **2004**, *381*, 363–371. [[CrossRef](#)]
30. Mishin, Y.; Mehl, M.J.; Papaconstantopoulos, D.A. Phase stability in the Fe–Ni system: Investigation by first-principles calculations and atomistic simulations. *Acta Mater.* **2005**, *53*, 4029–4041. [[CrossRef](#)]
31. Suryanarayana, C. Mechanical alloying and milling. *Prog. Mater. Sci.* **2001**, *46*, 1–184. [[CrossRef](#)]
32. Filho, J.B.; Kuhnlen, C.A. Electronic and Magnetic Structure of Ordered Fe-Ni Alloys. *Braz. J. Phys.* **1993**, *23*, 288–298.
33. Moravcik, I.; Cizek, J.; Zapletal, J.; Kovacova, Z.; Vesely, J.; Minarik, P.; Kitzmantel, M.; Neubauer, E.; Dlouhy, I. Microstructure and mechanical properties of Ni<sub>1.5</sub>Co<sub>1.5</sub>CrFeTi<sub>0.5</sub> high entropy alloy fabricated by mechanical alloying and spark plasma sintering. *Mater. Des.* **2017**, *119*, 141–150. [[CrossRef](#)]
34. Liang, Z.Y.; Huang, M.X. Deformation twinning in small-sized face-centred cubic single crystals: Experiments and modelling. *J. Mech. Phys. Solids* **2015**, *85*, 128–142. [[CrossRef](#)]
35. Kochmann, D.M.; Le, K.C. A continuum model for initiation and evolution of deformation twinning. *J. Mech. Phys. Solids* **2009**, *57*, 987–1002. [[CrossRef](#)]



© 2017 by the authors. Licensee MDPI, Basel, Switzerland. This article is an open access article distributed under the terms and conditions of the Creative Commons Attribution (CC BY) license (<http://creativecommons.org/licenses/by/4.0/>).